Energetics and Specificity of Interactions within Ub·Uev·Ubc13 Human Ubiquitin Conjugation Complexes †

ARTICLE *in* BIOCHEMISTRY · AUGUST 2003

Impact Factor: 3.02 · DOI: 10.1021/bi034480t · Source: PubMed

6 AUTHORS, INCLUDING:

Trevor F Moraes
University of Toronto
34 PUBLICATIONS **885** CITATIONS

SEE PROFILE

Wei Xiao
University of Saskatchewan
166 PUBLICATIONS **4,043** CITATIONS

SEE PROFILE

Energetics and Specificity of Interactions within Ub•Uev•Ubc13 Human Ubiquitin Conjugation Complexes†

Sean McKenna,‡ Jing Hu,‡ Trevor Moraes,‡ Wei Xiao,§ Michael J. Ellison,*,‡,∥ and Leo Spyracopoulos*,‡,∥

Department of Biochemistry, University of Alberta, Edmonton, Alberta T6G 2H7, Canada, Institute for Biomolecular Design, University of Alberta, Edmonton, Alberta T6G 2H7, Canada, and Department of Microbiology and Immunology, University of Saskatchewan, Saskatoon, Saskatchewan S7N 5E5, Canada

Received March 24, 2003; Revised Manuscript Received May 13, 2003

ABSTRACT: Lys^{63}-linked polyubiquitin (poly-Ub) chains appear to play a nondegradative signaling and/or recruitment role in a variety of key eukaryotic cellular processes, including NF-κB signal transduction and DNA repair. A protein heterodimer composed of a catalytically active ubiquitin-conjugating enzyme (Ubc13) and its homologue (Mms2 or Uev1a) forms a catalytic scaffold upon which a noncovalently associated acceptor Ub and thiolester-linked donor Ub are oriented such that Lys^{63}-linked poly-Ub chain synthesis is facilitated. In this study, we have used $^{1}H-^{15}N$ nuclear magnetic resonance spectroscopy, in combination with isothermal titration calorimetry, to determine the thermodynamics and kinetics of the interactions between various components of the Lys^{63}-linked poly-Ub conjugation machinery. Mms2 and Uev1a interact *in vitro* with acceptor Ub to form 1/1 complexes with macroscopic dissociation constants of 98 ± 15 and 213 ± 14 μM, respectively, and appear to bind Ub in a similar fashion. Interestingly, the Mms2•Ubc13 heterodimer associates with acceptor Ub in a 1/1 complex and binds with a dissociation constant of 28 ± 6 μM, significantly stronger than the binding of Mms2 alone. Furthermore, a dissociation constant of 49 ± 7 nM was determined for the interaction between Mms2 and Ubc13 using isothermal titration calorimetry. In connection with previous structural studies for this system, the thermodynamics and kinetics of acceptor Ub binding to the Mms2•Ubc13 heterodimer described in detail in this study will allow for a more thorough rationalization of the mechanism of formation of Lys^{63}-linked poly-Ub chains.

Protein ubiquitination is a key post-translational modification event for a variety of intracellular proteins involved in numerous degradative and regulatory pathways, including cell cycle control (*1*), NF-κB-dependent signal transduction (*2*, *3*), DNA repair (*4*, *5*), ribosome biogenesis (*6*), and endocytosis of cell surface proteins (*7*). The cellular protein ubiquitination machinery is responsible for the covalent formation of an isopeptide bond between the C-terminal carboxy group of ubiquitin (Ub)[1] and the ϵ-amino group of a solvent-exposed Lys on a target substrate. Covalent attachment of Ub to target substrates is accomplished by a series of three enzymes which may form high-energy thiolester linkages between an active site cysteine residue and the C-terminal carboxy group of Ub (*8*, *9*). Ub is initially activated by a highly conserved Ub activating enzyme (E1) that forms a thiolester adduct in an ATP- and Mg^{2+}-dependent manner. This is followed by transfer of the Ub molecule to the active site cysteine of a Ub conjugating enzyme (E2) *via* a transthiolesterification reaction. Substrate specificity is thought to be mediated by at least two families of Ub protein ligases (E3), which in combination with the E2 enzymes are responsible for the formation of an isopeptide bond between Ub and a Lys residue on the surface of the target.

Whereas a monoubiquitination event serves as a signal for certain cellular fates (*10*), in most cases, one observes formation of poly-Ub chains on the target substrate through repetitive conjugation of Ub molecules to each other (*11*). The Ub molecules are linked to each other through an isopeptide bond formed between the C-terminal carboxy group of an incoming, or donor, Ub and one of seven lysine residues on the surface of a substrate-attached, or acceptor, Ub. As a result, a variety of poly-Ub chains defined by the Lys residue linking sequential Ub molecules exist, and these chains likely adopt unique topologies, and therefore poten-

† This work was supported by the Canadian Institutes of Health Research (CIHR), the National Cancer Institute of Canada (NCIC), and the Alberta Heritage Foundation for Medical Research (AHFMR). S.M. is supported by Natural Sciences and Engineering Research Council of Canada (NSERC), AHFMR, and Izaak W. Killam studentships. J.H. is supported by an AHFMR studentship. T.M. is supported by CIHR and AHFMR studentships.

* To whom correspondence should be addressed. L.S.: e-mail, leo.spyracopoulos@ualberta.ca; telephone, (780) 492-2417; fax, (780) 492-0886. M.J.E.: e-mail, mike.ellison@ualberta.ca; telephone, (780) 492-6352; fax, (780) 492-0886.

‡ Department of Biochemistry, University of Alberta.

§ University of Saskatchewan.

∥ Institute for Biomolecular Design, University of Alberta.

[1] Abbreviations: $^{1}H-^{15}N$ HSQC, $^{1}H-^{15}N$ heteronuclear single-quantum coherence; BCA, bicinchoninic acid; DSS, 2,2-dimethyl-2-silapentane-5-sulfonate; DTT, dithiothreitol; E1, ubiquitin-activating enzyme; E2, ubiquitin-conjugating enzyme; E3, ubiquitin-protein ligase; EDTA, ethylenediaminetetraacetic acid; HEPES, *N*-(2-hydroxyethyl)-piperazine-*N*′-2-ethanesulfonic acid; ITC, isothermal titration calorimetry; K_D, macroscopic dissociation constant; NMR, nuclear magnetic resonance; SDS−PAGE, sodium dodecyl sulfate−polyacrylamide gel electrophoresis; Uev, ubiquitin-conjugating enzyme variant; Ub, ubiquitin.

10.1021/bi034480t CCC: $25.00
Published on Web 06/12/2003

tially different functional roles (*12*−*17*). Poly-Ub chains linked through Lys^{48} are the best understood; this chain configuration typically targets proteins for degradation *via* the 26S proteasome and therefore serves an obviously crucial role in the regulation of cellular protein levels (*8*). The alternative covalent tethering of Lys^{63}-linked Ub chains to a target substrate, on the other hand, serves not as a proteolytic tag for the target but instead as a recruitment and/or signaling marker. The importance of Lys^{63}-linked chains is underscored by their role in both NF-κB (*3*, *18*) signaling and error-free postreplicative DNA repair processes (*5*, *19*−*22*).

The catalytic mechanisms through which specific poly-Ub chain linkages are assembled and delivered to substrates are poorly understood. Surprisingly, some of the first insights into these processes have come not from well-characterized systems involving the assembly of Lys^{48} poly-Ub chains but from the study of noncanonical Lys^{63} poly-Ub linkages. Lys^{63}-linked poly-Ub chains are assembled through a conserved heterodimer of E2 proteins composed of a catalytically active Ubc13 subunit and an inactive E2-like subunit, or Ub conjugating enzyme variant (Uev) (*23*). Uev proteins share significant sequence and structural similarities with E2s (*24*, *25*), yet lack the requisite active site cysteine required for thiolester formation. Structurally, it appears as though the Mms2•Ubc13 heterodimer serves as a binding scaffold for two Ub molecules: a primarily Mms2-associated "acceptor" Ub and a thiolester-linked "donor" Ub on Ubc13 (*24*−*27*). A model of the tetrameric complex, based on NMR chemical shift mapping, reveals that this orientation not only favors the formation of Lys^{63}-linked chains through the proximal positioning of Lys^{63} on the acceptor Ub and C-terminus of the donor Ub tethered to the Ubc13 active site but also precludes the formation of Lys^{48}-linked chains, as this residue is buried in the acceptor Ub•Mms2 interface (*26*, *27*). Therefore, structural studies have allowed us to define a structural rationale for the assembly of specific poly-Ub chain linkages. However, a complete picture for this mechanism necessarily involves unraveling the thermodynamics and kinetics of the underlying protein−protein interactions.

In this study, we examined the thermodynamics and kinetics of the interactions within the Uev•Ubc13•Ub_2 tetramer using a combination of nuclear magnetic resonance (NMR) chemical shift titration and isothermal titration calorimetry (ITC) experiments. This approach has allowed for estimation of the affinity, stoichiometry, specificity, and kinetics of binding between the acceptor Ub and (i) Mms2, (ii) Mms2•Ubc13, or (iii) Uev1a, as well as between the E2-Uev heterodimer components (Mms2 and Ubc13). The results are crucial for understanding the thermodynamic and kinetic aspects of complex assembly, understanding binding differences between Uev proteins, and confirming the validity of the previously determined model for the tetrameric complex (*26*). Combined with our previous work, a more complete mechanism for poly-Ub chain formation has been determined, and may serve as a more general mechanism for different poly-Ub chain linkages.

EXPERIMENTAL PROCEDURES

Protein Expression. Cloning, expression, and purification of ^{15}N-labeled and unlabeled hMms2, hUbc13, Ub, and E1 were performed as described previously (*26*, *27*). Human Uev1a was purified as a GST fusion protein and subsequently cleaved from GST in a manner identical to that previously described for Mms2 (*27*), with the exception that cleavage of the GST moiety proceeded for 4 h, and protease inhibitors (Calbiotech, set II cocktail) were then immediately added. It should be noted that for hMms2, hUev1a, and hUbc13 proteins, cleavage of the GST moiety leaves a five-residue linker attached to the N-terminus of the recombinant protein. SDS−PAGE analysis, bicinchoninic acid (BCA) protein assays, and amino acid analyses were employed to confirm the concentration and purity of the samples prior to and during the titration experiments.

NMR Samples. All NMR sample volumes were approximately 500 μL (90% H_2O and 10% D_2O) prior to titration, and included 50 mM HEPES (pH 7.5), 150 mM NaCl, 1 mM EDTA, 10 mM DTT, and 1 mM 2,2-dimethyl-2-silapentane-5-sulfonate (DSS, internal ^1H chemical shift standard). The pH of the samples was adjusted to 7.5.

NMR Spectroscopy. All NMR spectra were obtained using a Varian Unity INOVA 600 MHz spectrometer operating at 30 °C. The two-dimensional (2D) $^1H-^{15}N$ HSQC NMR spectra were acquired using the sensitivity-enhanced gradient pulse scheme developed by Kay and co-workers (*28*, *29*). The ^1H and ^{15}N sweep widths were 8000 and 2200 Hz, respectively. A minimum of 64 transients per point in the indirect (^{15}N) dimension were collected for each spectrum. Spectral processing was accomplished with NMRPipe (*30*). NMRview (*31*) was employed in the assignment of all 2D $^1H-^{15}N$ HSQC NMR cross-peaks.

Titration of [^{15}N]Mms2 with Ub. To an NMR sample containing 500 μM [^{15}N]Mms2 were successively added 15 μL aliquots of 6.5 mM Ub for a total of nine titration points. For all titrations carried out in this study, following acquisition of a 2D $^1H-^{15}N$ HSQC NMR spectrum for each titration point, up to 5 μL of the NMR sample was set aside for use in duplicate amino acid analyses, giving [Ub]/[[^{15}N]Mms2] ratios of 0, 0.33, 0.65, 0.98, 1.31, 1.65, 1.98, 2.32, 2.67, and 3.01 for the respective titration points. While this technique did result in significant volume increases, changes in concentration for both titrant and analyte were taken into account in the final analysis for all titrations presented herein. The pH of the sample was routinely checked, and maintained at 7.5 throughout this and all titrations conducted in this study. For all titrations, a one-dimensional (1D) ^1H NMR spectrum was acquired prior to each 2D $^1H-^{15}N$ HSQC NMR spectrum to assess potential salt-dependent changes in the ^1H pulse width. The pulse width remained unchanged from its initial value (7.0 μs) for this and all other titrations presented herein.

Titration of [^{15}N]Uev1a with Ub. To an NMR sample containing 130 μM [^{15}N]Uev1a were successively added 10, 10, 15, 15, 15, 15, 20, and 20 μL aliquots of 2.8 mM Ub for a total of nine titration points. For the respective titration points, [Ub]/[[^{15}N]Uev1a] ratios of 0, 0.36, 0.72, 1.27, 1.82, 2.38, 2.95, 3.71, and 4.47 were obtained from amino acid analyses.

Titration of [^{15}N]Mms2•Ubc13 with Ub. To an NMR sample containing 151 μM [^{15}N]Mms2•Ubc13 were successively added 10, 10, 5, 10, and 7.5 μL aliquots of 3.6 mM Ub for a total of five titration points, corresponding to [Ub]/[[^{15}N]Mms2•Ubc13] ratios of 0, 0.44, 0.89, 1.11, 1.55, 1.89, and 2.20.

Titration of [^{15}N]Ubc13 with Mms2. Successive aliquots of 10, 10, 5, 10, and 7.5 μL of 950 μM Mms2 were added to an NMR sample containing 344 μM [^{15}N]Ubc13 for a total of five titration points. [Mms2]/[[^{15}N]Ubc13] molar ratios of 0, 0.12, 0.23, 0.35, 0.48, 0.61, 0.79, 0.91, 1.09, and 1.27 were obtained from amino acid analyses for the respective titration points.

Calculation of Dissociation Constants. Dissociation constants were determined by following changes in backbone amide $^{1}H_N$ and ^{15}N chemical shifts for Uev proteins in 2D $^{1}H-^{15}N$ HSQC NMR spectra upon addition of ligand. The total average change in backbone amide chemical shifts for the entire protein for each point in a titration was calculated using the following equation (*32*):

$$\Delta\delta_{total} = \frac{\sum_{j=1}^{n}\sqrt{(\Delta\delta^{15}N_j)^2 + (\Delta\delta^{1}H_{Nj})^2}}{n} \quad (1)$$

where $\Delta\delta^{15}N_j$ and $\Delta\delta^{1}H_{Nj}$ are the chemical shift changes in hertz for residue j, and the summation extends over all residues ($j = 1-n$) that were employed in the calculation. The average change in total chemical shift was calculated at the end point of the titration using each of the residues whose chemical shifts changed significantly during titration, and the fractional change in total chemical shift was determined for each titration point by normalization to the end point $\Delta\delta_{total}$. This value was then plotted as a function of the ligand/protein molar ratio and fit to eq 2, to yield a macroscopic dissociation constant ($K_D = k_{off}/k_{on}$) for the interaction between a protein (P) and ligand (L):

$$[PL] = {}^{1}/_{2}[K_D + [L]_0 + [P]_0 - \sqrt{(K_D + [L]_0 + [P]_0)^2 - 4[L]_0[P]_0}] \quad (2)$$

where K_D is the dissociation constant, $[P]_0$ is the total protein concentration, $[L]_0$ is the total ligand concentration, and [PL] is the concentration of the protein−ligand complex (*33*). K_D was determined from $\Delta\delta_{total}$ through a nonlinear least-squares fit using the program Xcrvfit (available at http://canopus-.pence.ualberta.ca/ftp/).

Line Shape Analysis for Determination of Off-Rate Constants. Cross-peaks in 2D $^{1}H-^{15}N$ HSQC NMR spectra during titration of Ub into either [^{15}N]Mms2 or [^{15}N]Uev1a fall into the limit of fast exchange on the NMR time scale, and therefore appear as single resonances that move progressively toward the bound chemical shifts upon addition of Ub according to

$$\delta_{obs} = (1 - P_b)\delta_f + P_b\delta_b \quad (3)$$

where δ_{obs} is the observed chemical shift of the backbone amide cross-peak, P_f and P_b are the free and bound fractions of Mms2, respectively, and δ_f and δ_b are the chemical shifts for the free and bound species, respectively (*32*). Mathematica (*34*) was used to simulate ^{1}H NMR line shapes using the experimentally derived values of $\Delta\upsilon_f$ (line width at half-height for free protein), $\Delta\upsilon_b$ (line width at half-height for bound protein), δ_f, δ_b, and K_D, adjusting k_{off} manually, and using the equations describing effects of site exchange on NMR spectra (*32*, *35*).

Isothermal Titration Calorimetry of Mms2·Ubc13. A VP-ITC microcalorimeter (Microcal, Northampton, MA) was used to analyze binding of Mms2 and Ubc13. Proteins were dialyzed against 50 mM Tris (pH 7.5), 150 mM NaCl, and 1 mM ETDA and degassed prior to analysis. Ubc13 (7 μM) was injected into the sample cell, and Mms2 (70 μM solution) was placed into the syringe, or vice versa with the exception that a slightly higher concentration of analyte was used (80 μM). The dialysis buffer was placed in the reference cell. Either Mms2 or Ubc13 was titrated against dialysis buffer to obtain the heat of dilution. The following parameters were used in the titration: 30 °C, 10 μL injections, and 4 min between injections with stirring at 305 rpm. These titration data were fit using Microcal Origin (version 5.0) to extract thermodynamic parameters.

RESULTS

Ub Binding to Uev Proteins. (a) Interaction of Ub with Mms2. Examination of the thermodynamics and kinetics of the interaction between noncovalently bound acceptor Ub and the Ubc13·Uev scaffold involved analysis of 2D $^{1}H-^{15}N$ HSQC NMR spectra for [^{15}N]Mms2 in the free state and upon successive additions of unlabeled Ub (Figure 1A). This scheme allowed for monitoring of the NMR resonance peaks for the [^{15}N]Mms2 component without interference from unlabeled Ub NMR resonance peaks. The 2D $^{1}H-^{15}N$ HSQC NMR spectrum of [^{15}N]Mms2 alone shows approximately 120 backbone amide cross-peaks which can be used to follow the titration with Ub in detail. Changes in cross-peak resonance frequencies can reflect changes in the local chemical environment, and therefore identify residues which are potentially involved in the interaction with Ub.

Contour plots of the $^{1}H-^{15}N$ HSQC NMR spectra recorded during titration of Ub into [^{15}N]Mms2 are shown in Figure 1A. Eighteen backbone amide $^{1}H_N-^{15}N$ cross-peaks, corresponding to residues Glu^{21}, Gly^{22}, Gly^{25}, Val^{26}, Gly^{29}, Thr^{30}, Val^{31}, Ser^{32}, Gly^{34}, Thr^{47}, Gly^{48}, Met^{49}, Gly^{52}, Asn^{60}, Tyr^{63}, Lys^{65}, Val^{117}, and Gln^{120}, were observed to experience significant changes in chemical shift upon addition of Ub, indicating possible participation in the interface between Mms2 and acceptor Ub. These residues cluster to the α1 and α2 helices, and the first three β-strands of Mms2. These residues map to a concave surface on one face of the protein (Figure 2A). These results are in good agreement with previous chemical shift perturbation studies which delineated the surfaces of interaction between the protein species (*26*).

On the basis of previous biochemical and NMR data (*26*, *27*), the noncovalent interaction between Ub and a given Uev is expected to be weak (K_D in the micromolar range). In accordance with this expectation, all of the backbone amide chemical shift changes fall into the fast exchange limit on the NMR time scale to a first approximation (see line shape analysis below), as is often observed for weaker interactions (*36*). At any given point during the titration, only a single set of cross-peaks, whose chemical shifts are the weighted average of the free and bound chemical shifts, are observed. The linear trajectories for the shifting cross-peaks in the 2D $^{1}H-^{15}N$ NMR spectra for [^{15}N]Mms2 are indicative of a 1/1 weak interaction between Ub and Mms2.

Residues that undergo backbone amide $^{1}H_N$ or ^{15}N chemical shift changes during the titration can be monitored to

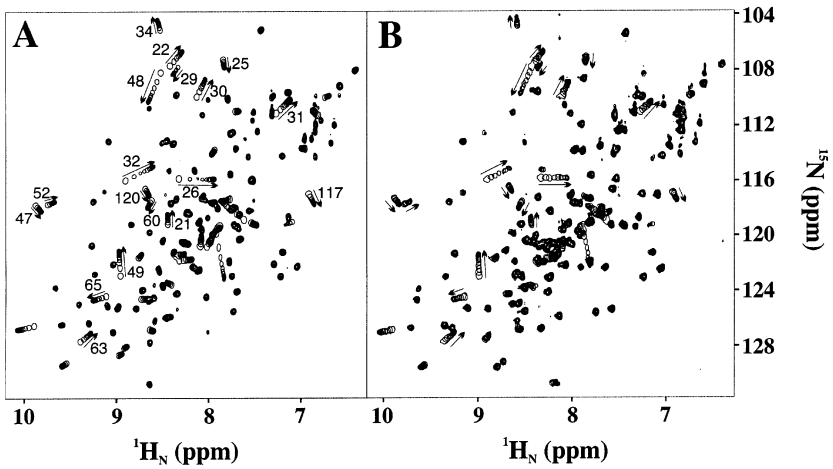

FIGURE 1: Contour plots of 2D $^1H-^{15}N$ HSQC NMR spectra from the backbone amide regions of ^{15}N-labeled Mms2 (A) or Uev1a (B), showing the effect of Ub addition. The final titration point in each spectrum is shown as multiple contours, whereas all other points are represented by a single contour. The well-resolved cross-peaks which undergo significant changes in chemical shift during titration are numbered according to residue, with the progress of the titration labeled with an arrow. Only those residues labeled with arrows were used in the analysis of the K_D value.

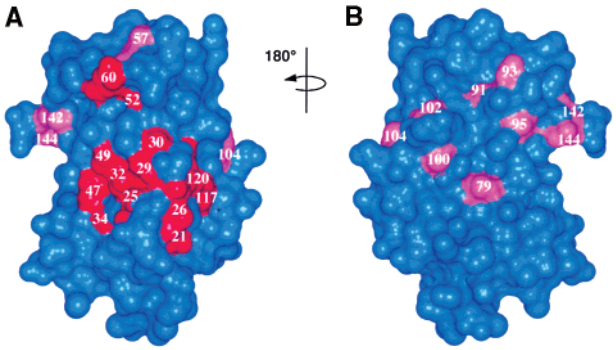

FIGURE 2: Ub binding site on the surface of Mms2. The surface of Mms2 (blue) is presented, showing the putative acceptor Ub interaction site. Residues affected by noncovalent interaction with Ub, as determined by 2D $^1H-^{15}N$ HSQC NMR chemical shift titrations (Figure 1), are colored red. Nonidentical residues between Mms2 and Uev1a are colored purple. Note that these nonidentical residues occur at regions of the protein surface different from those involved in Ub binding.

quantitate the thermodynamics and kinetics of binding between two protein species. The fractional change in total chemical shift was determined for each titration point, and these values were plotted as a function of the [Ub]/[[^{15}N]-Mms2] ratio and fit to eq 2 with P being Mms2 and L being Ub, yielding a macroscopic dissociation constant (K_D) of 98 ± 15 μM for a 1/1 binding complex [Figure 3A (♦)]. The completeness of the titration is evidenced by the fact that the chemical shifts for all 18 cross-peaks undergoing significant changes during Ub titration cease to do so at an approximate 3-fold excess of Ub over Mms2. Furthermore, the dependence of backbone amide Mms2 chemical shifts upon Ub concentration for each of the cross-peaks whose chemical shifts change significantly upon titration is virtually identical, consistent with a single binding event.

One-dimensional traces through the ^1H dimension for numerous cross-peaks for the 2D $^1H-^{15}N$ HSQC spectrum of [^{15}N]Mms2 were recorded, and a representative trace corresponding to the backbone amide resonance of Val^{26} is shown in Figure 3B (top) to display the effect of exchange between free and Ub-bound Mms2 at various points during the titration. For the backbone amide resonance of Val^{26}, the total change in chemical shift in the ^1H dimension is 230 Hz, and significant line broadening is observed during the titration, but the resonance peak sharpens dramatically when [^{15}N]Mms2 is saturated with Ub. This broadening phenomenon is expected because the effect of chemical exchange on line width is dependent upon the chemical shift difference between the free and bound states:

$$\Delta\upsilon_{ex} = P_f P_b \tau_{ex} (\delta_f - \delta_b)^2 \quad (4)$$

where $\Delta\upsilon_{ex}$ is the observed line width, P_f and P_b are the free and bound [^{15}N]Mms2 fractions, respectively, and τ_{ex} is the exchange lifetime defined as $(\tau_f\tau_b)/(\tau_f + \tau_b)$. Computer simulations of the observed line shape changes were performed using the experimentally derived values of $\Delta\upsilon_f$, $\Delta\upsilon_b$, δ_f, δ_b, and K_D and manually adjusting k_{off}. A k_{off} value of 2250 ± 500 s^{-1} provides a satisfactory fit with the experimental data (Figure 3B, bottom).

(b) Interaction of Ub with Uev1a. The sequence of Uev1a, a homologue of Mms2 involved in NF-κB signaling, is highly identical (92%) within the core Uev domain (residues 1−145 of Mms2), but not with the N-terminal extension or 11 scattered amino acid substitutions throughout Uev1a (Figure 4A). Whereas the noncovalent interaction between Ub and Mms2 has been well characterized (*26*, *27*), there is scant information regarding a potential noncovalent interaction between Uev1a and Ub, as well as the potential differences and/or similarities between its mode of Ub binding and that of Mms2.

The 2D $^1H-^{15}N$ HSQC NMR spectrum for [^{15}N]Uev1a is shown in Figure 4B (red contours). The backbone amide resonances show the line width and dispersion expected for an E2-like protein, with the exception of a cluster of cross-peaks found at chemical shifts typical of random coil secondary structure. Although we have not assigned the backbone amide chemical shifts for [^{15}N]Uev1a, it is apparent that upon superposition with the 2D $^1H-^{15}N$ HSQC NMR spectrum of [^{15}N]Mms2 (Figure 4B, black contours) the chemical shifts for the backbone amide cross-peaks for the two proteins are similar. Notable exceptions are the residues that presumably correspond to the N-terminal extension of

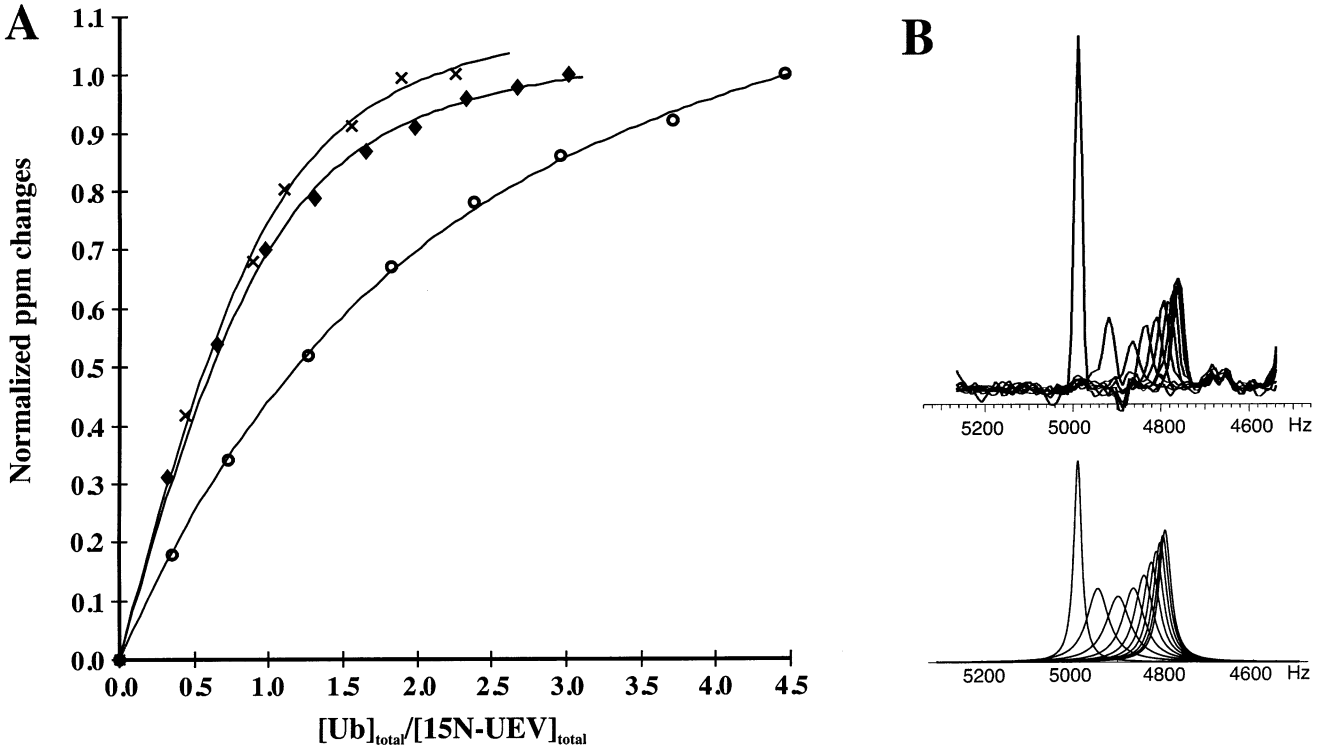

FIGURE 3: (A) Binding curves derived from 2D ^{1}H−^{15}N HSQC NMR titrations of Ub into [^{15}N]Mms2 (♦), [^{15}N]Uev1a (○), and [^{15}N]-Mms2·Ubc13 (×). The average normalized changes (parts per million) are plotted as a function of the [Ub]/[^{15}N-labeled species] ratio, with nonlinear least-squares fits to the data shown as solid lines. The errors in the data points are smaller than the size of the corresponding symbols. (B) 1D ^{1}H traces taken through the cross-peaks of Val^{26} from 2D ^{1}H−^{15}N HSQC NMR spectra during titration of Ub into [^{15}N]-Mms2 (top). The corresponding line shape simulation using a k_{off} value of 2250 s^{-1} is also shown (bottom).

Uev1a which is likely disordered in solution, and those which are nonidentical in the primary amino acid sequence. The disordered conformation of the N-terminal extension for Uev1a likely results in both the difficulty in crystallizing the full-length species and its susceptibility to proteolysis during purification (T. Moraes, personal communication). Given the level of sequence identity of 92% for Mms2 and Uev1a for the core domain residues, and the similarity for the 2D ^{1}H−^{15}N HSQC NMR spectra, we conclude that the structures of Mms2 and Uev1 are likely to be similar.

2D ^{1}H−^{15}N HSQC NMR spectra were collected for [^{15}N]-Uev1a in the free state and upon successive addition of unlabeled Ub. Contour plots of the spectra during titration with Ub are shown in Figure 1B. Of the 135 backbone amide cross-peaks that can be used to follow the titration of Ub into Uev1, 18 of these cross-peaks were observed to shift in a linear fashion upon successive additions of Ub, and fall into the fast exchange limit on the NMR time scale. Upon inspection of the 2D ^{1}H−^{15}N HSQC NMR spectrum of free [^{15}N]Uev1a, it is clear that many of the resonances superimpose with those in the spectrum of free [^{15}N]Mms2 (Figure 4B), indicating that the chemical shift assignments for Uev1a are likely to be similar to those for Mms2. Furthermore, the trajectories for resonances in Uev1a undergoing significant changes in chemical shift upon titration with Ub match well those observed in Mms2, indicating that a similar binding interface is used by each protein with respect to Ub binding (Figure 1). To complement this result, the surface on Ub involved in binding Uev1a, as determined from chemical shift perturbation experiments with [^{15}N]Ub (data not shown), is similar to that found previously for the interaction between [^{15}N]Ub and Mms2 (*27*). Therefore, we conclude that the weak noncovalent interaction between Ub and Uev1a likely employs a mode of binding similar to that of Ub binding to Mms2.

To quantitatively compare the thermodynamics and kinetics of Ub binding between Mms2 and Uev1a, the average fractional change in total chemical shift was calculated on the basis of the 18 residues labeled in Figure 1B, plotted as a function of the [Ub]/[[^{15}N]Uev1a] ratio, and fit to eq 2 with P being Uev1a and L being Ub, giving a K_D value of 213 ± 14 μM for a 1/1 complex [Figure 3A (○)]. As is the case for Mms2, the rate and linearity for the trajectory of movement for each of the significant cross-peaks are virtually identical, indicating a single binding event requiring an approximate 4.5-fold excess of Ub to saturate Uev1a. However, the observed K_D is 2.2-fold larger than that for the interaction between Ub and Mms2, indicating a weaker interaction despite the fact that presumably similar residues are implicated in the binding event.

One-dimensional traces through numerous cross-peaks of Uev1a were recorded, and computer simulations of the experimental line shapes were performed using the experimentally derived values of $\Delta\nu_f$, $\Delta\nu_b$, δ_f, δ_b, and K_D and adjusting k_{off} manually. A k_{off} of 1800 ± 450 s^{-1} provides a satisfactory fit with the experimental data (data not shown), indicating a slight difference compared to that for the Ub·Mms2 interaction.

Interaction of Ub with the Mms2·Ubc13 Heterodimer. The heterodimerization of Mms2 (or Uev1a) with Ubc13 is a prerequisite for the synthesis of Lys^{63}-linked poly-Ub chains. Therefore, determination of the thermodynamics and kinetics of interaction between Ub and the Mms2·Ubc13 heterodimer is important in understanding the contribution that Ubc13

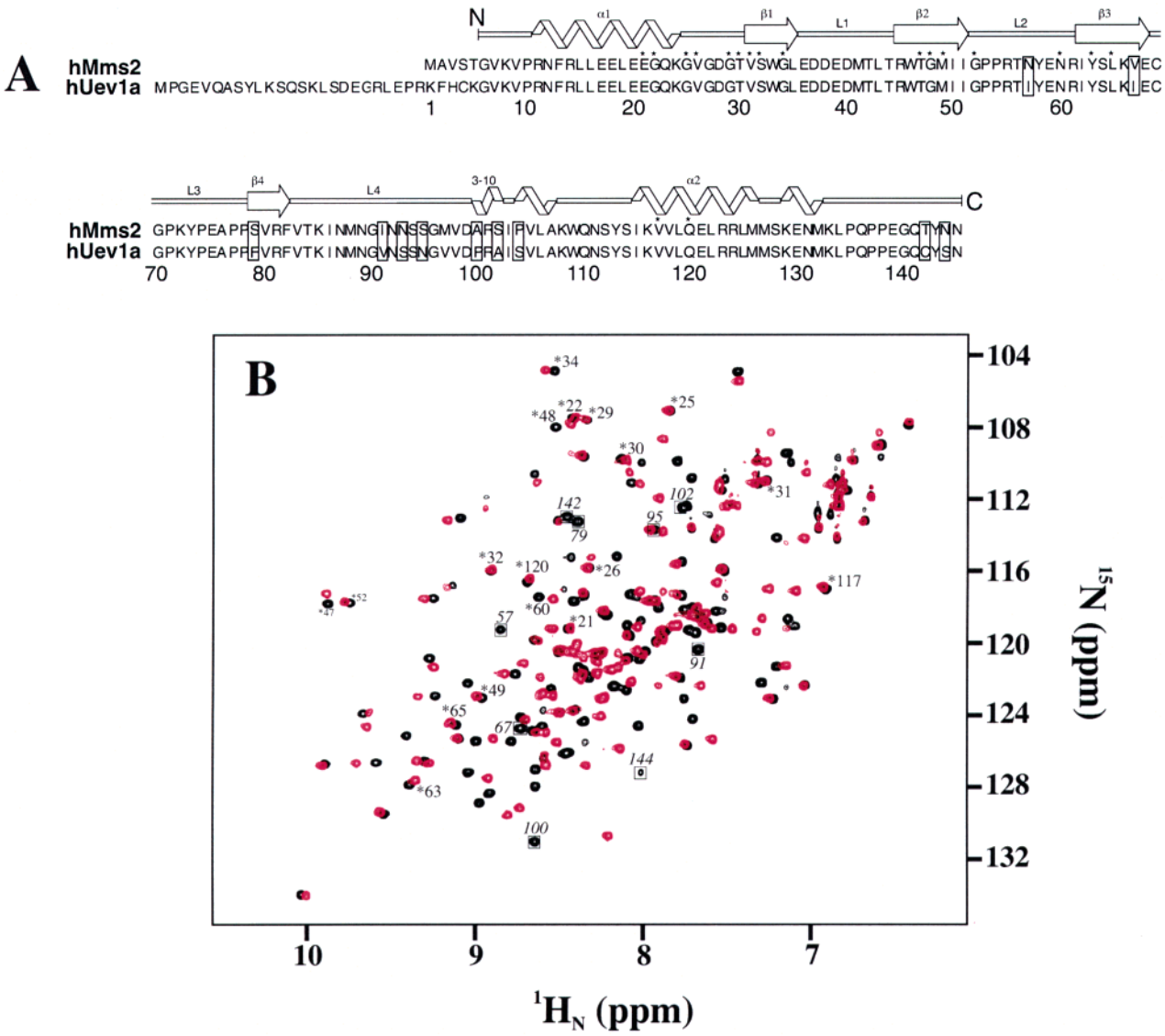

FIGURE 4: (A) Sequence alignment of human Mms2 and Uev1a, shown with the corresponding secondary structures (*24*). Important residues are labeled as described below. (B) Superposition of 2D ^{1}H−^{15}N HSQC NMR spectra of free [^{15}N]Mms2 (black) and [^{15}N]Uev1a (red). Cross-peaks in [^{15}N]Mms2 which are affected by complex formation with Ub are numbered and denoted with an asterisk, while those which differ between the Uevs are numbered and boxed.

makes to noncovalent acceptor Ub binding. This is of particular interest in light of the fact that Mms2 alone makes extensive noncovalent interactions with Ub, while Ubc13 alone has no detectable affinity for Ub molecules (*27*). In employing solution NMR to analyze the interaction of Ub with the Mms2•Ubc13 heterodimer, we find that a complicating factor is the increase in molecular mass for the complex (42.5 kDa) relative to that of Mms2 and Ub alone (25.5 kDa), which results in a decrease in the signal-to-noise ratio for 2D ^{1}H−^{15}N HSQC NMR spectra. Furthermore, certain backbone amide cross-peak resonances for [^{15}N]-Mms2 change and/or disappear upon heterodimerization, and cannot be identified for the analysis.

Titration of Ub into the Mms2•Ubc13 heterodimer employed an NMR sample for which only Mms2 was labeled with ^{15}N, thereby simplifying the spectrum. 2D ^{1}H−^{15}N HSQC NMR spectra were collected for the [^{15}N]Mms2•Ubc13 complex free of Ub, and upon successive additions of unlabeled Ub. Of the 105 observable backbone amide cross-peaks, 16 were observed to shift significantly: Glu^{21}, Gly^{22}, Val^{26}, Gly^{29}, Thr^{30}, Val^{31}, Ser^{32}, Gly^{34}, Thr^{47}, Gly^{48}, Met^{49}, Gly^{52}, Asn^{60}, Tyr^{63}, Lys^{65}, and Gln^{120}. Each of these peaks moved in a linear fashion upon titration with Ub, and exhibited fast exchange on the NMR time scale. These 16 residues correspond to those involved in the interaction between Ub and the Mms2 subunit alone (see above), indicating that a similar mode of binding between Mms2 and Ub is employed in the heterodimer. This result is in agreement with previous chemical perturbation experiments (*26*).

To quantitate the thermodynamics and kinetics of Ub binding to Mms2 within the heterodimer, the average fractional change in total chemical shift was calculated on the basis of the 16 residues described above, plotted as a function of the [Ub]/[[^{15}N]Mms2•Ubc13] ratio, and fit to eq 2 with P being [^{15}N]Mms2•Ubc13 and L being Ub, to give a K_D of 28 ± 6 μM [Figure 3A (×)]. As is the case with binding of Ub to Mms2 alone, the rate of the trajectory of movement for each of the significant cross-peaks is virtually identical, indicating a single binding event requiring an

approximate 2-fold excess of Ub for saturation of Mms2. The observed K_D is 3.5-fold smaller than that for the interaction between Ub and Mms2 alone, indicating a greater affinity of Ub for Mms2 within the heterodimer. We therefore conclude that Ubc13 contributes to the thermodynamics and kinetics of Ub binding within the Mms2•Ubc13 heterodimer (see the Discussion).

A line shape analysis for the determination of a k_{off} value was not possible due to a reduced signal-to-noise ratio for the spectra of the Ub•[^{15}N]Mms2•Ubc13 heterotrimer compared to that for the spectra of the Ub•[^{15}N]Mms2 heterodimer.

Thermodynamics of the Interaction between Components of the Mms2•Ubc13 Heterodimer. Mms2 and Ubc13 form a stable heterodimer over a range of concentrations and solution conditions (*26*, *27*). An upper limit to K_D for the heterodimer of 2 μM was previously determined by analytical ultracentrifugation (*24*). The high-affinity limit for quantitative determination of the dissociation constant by solution NMR currently lies around 3 μM (*36*, *37*). A 2D ^{1}H$-^{15}$N HSQC NMR titration experiment in which Ubc13 was labeled ^{15}N and unlabeled Mms2 was used as the titrant was performed to determine a K_D for the Ubc13•Mms2 interaction. The K_D value was estimated to be 1 ± 1 μM. However, because of the poor fit of the data, this value should be treated as an upper limit. It is worth noting that the chemical shift change maximum occurred between [Mms2]/[[^{15}N]Ubc13] molar ratios of 0.91 and 1.09, indicating the formation of an equimolar complex of the two proteins at a molar ratio of close to 1/1.

To more accurately probe the thermodynamics of the heterodimer interaction, isothermal titration calorimetry (ITC) was employed (Figure 5). ITC experiments were conducted in which the reaction cell contained either Ubc13 or Mms2, and small equivalent volume injections of the complementary heterodimer component were progressively added. The heat evolved upon binding is monitored as the titrant is successively injected, allowing for the calculation of thermodynamic parameters. This analysis yielded an average K_D of 49 ± 7 nM for the interaction between heterodimer components ($\Delta H = -5946 \pm 59$ cal/mol, $\Delta S = 13.8 \pm 2.3$ cal mol^{-1} °C^{-1}).

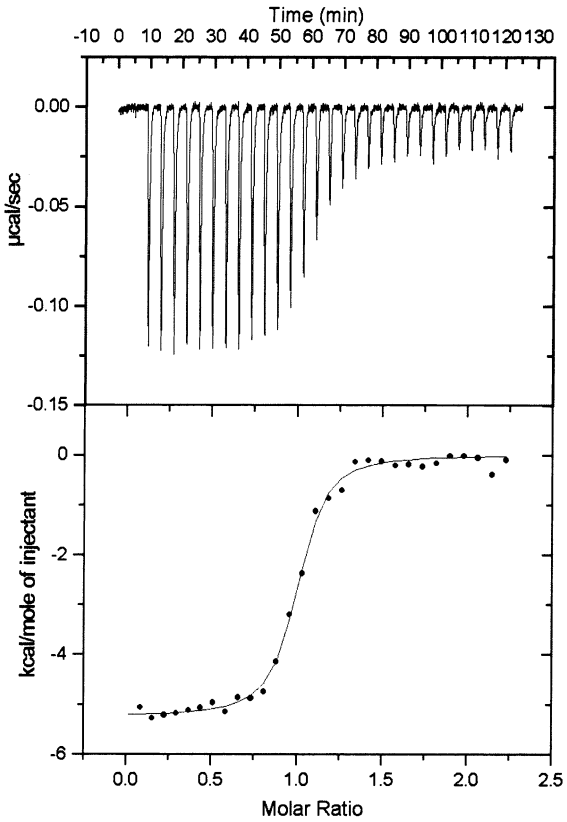

FIGURE 5: ITC thermogram for titration of Ubc13 (7 μM, sample cell) with Mms2 (70 μM, syringe), with the heat evolved shown on a per injection basis (top). ITC titration curve for the same reaction (bottom), where the heat evolved per injection is shown as a function of the molar ratio of Mms2 to Ubc13.

DISCUSSION

Central issues regarding the mechanism responsible for the formation of Lys^{63}-linked poly-Ub chains by the Mms2•Ubc13 heterodimer are the structural features which enable the heterodimer to perform its catalytic function and the thermodynamics and kinetics of the interactions between donor and acceptor Ub moieties and the heterodimer scaffold. Backbone amide chemical shift perturbation analysis has allowed the construction of a low-resolution model of the interactions between the Mms2•Ubc13 scaffold and two molecules of Ub (the acceptor Ub bound noncovalently primarily by Mms2 and a thiolester-linked donor Ub on Ubc13), which predicts a reasonable mechanism in which Lys^{63} of the acceptor Ub is placed in the proximity of both Gly^{76} of the donor Ub and the active site Cys^{87} on Ubc13 (*26*). Here we report the affinity, stoichiometry, specificity, and kinetics of interaction between various members of the tetrameric complex, as determined using 2D ^{1}H$-^{15}$N HSQC NMR titration experiments and isothermal titration calorimetry. The results are important with respect to gaining an understanding of the thermodynamics and kinetics associated with the poly-Ub chain building mechanism.

The thermodynamics and kinetics of Ub binding to two human Uev proteins, Mms2 and Uev1a, were examined in detail and illustrated striking similarities and some subtle differences between their modes of binding. As expected, both Mms2 and Uev1a bind Ub noncovalently in a 1/1 stoichiometry, and use virtually identical residues to mediate the binding event (Figure 1). Uev contacts with Ub involve residues from the N-terminal α-helix, the first three stands of the β-sheet, and the C-terminal α-helix, which correspond well with those residues previously determined to be important in the Mms2−Ub interaction (*26*). When mapped onto the surface of the known Mms2 structure (*24*), these residues cluster to a single concave surface of the molecule with an area appropriate for Ub binding (Figure 2A). However, Mms2 binds Ub with a 2.2-fold higher affinity than Uev1a, indicating that despite the use of a similar binding surface, subtle differences in terms of the binding interface with Ub may exist. Whereas the majority of the amino acid differences between these two proteins cluster to a surface on the protein opposite that responsible for Ub binding (Figure 2B), a few key differences, including Asn^{57}-Ile, Val^{67}Ile, Phe^{104}Ser, Thr^{142}Cys, and Asn^{144}Ser substitutions and the 25-residue N-terminal extension, may account for the difference in affinity for Ub between the Uevs (Figure 4A). It is also important to consider the fact that we are looking exclusively at changes in local environment for the

backbone amide bond and not directly at side chain structural interactions, which may prove to be more informative. Furthermore, the difference between the two Uev proteins in affinity for Ub could be minimized upon heterodimerization with Ubc13, though there are not data to support this possibility. Regardless, the K_D values that are determined are reasonable, and likely support the interaction *in vivo* despite the relatively weak binding that is observed. The mechanism of chain formation would require efficient release of Ub_2 from the Ubc13•Mms2 heterodimer, necessitating a weak interaction. It should be noted that the interaction with additional protein factors (i.e., E3 proteins) may also modulate the affinity for Ub.

The results presented herein are corroborated by the fact that another Uev, Tsg101, binds Ub noncovalently with a K_D of approximately 600 μM, though the structural basis for this interaction is distinct from that between Mms2 and Ub (*38*). While Mms2 and Uev1a each serve to properly orient Ub to achieve synthesis of Lys^{63}-linked poly-Ub chains, the cellular pathways in which they are involved are different. Preliminary results have also indicated that Uev1a and Mms2 have different *in vitro* chain building activities.[2] Taken together, these results imply that the different affinities for Ub between these proteins are important in Ub binding and/or release and thus must account in part for differences in poly-Ub chain building catalyzed by the two proteins.

Previous studies have demonstrated that the Ubc13 subunit alone has no detectable affinity for Ub under conditions and at concentrations that are appropriate for NMR (*26*, *27*). Furthermore, Mms2 binds Ub specifically, regardless of its state of heterodimerization with Ubc13. We therefore sought to examine in detail whether heterodimerization of Mms2 significantly affects the thermodynamics and kinetics of Ub binding. It was determined that Ub is bound 3.5-fold more tightly by the Mms2•Ubc13 heterodimer than by the Mms2 subunit alone, and that Mms2 and Ubc13 interact in a 1/1 stoichiometry. This result is striking given that similar residues on the surface of Mms2 within the heterodimer appear to be involved in complex formation. On the basis of these results, it is clear that either the interaction with Ubc13 modulates the Mms2 binding interface or Ubc13 is involved in directly binding the acceptor Ub molecule. The latter conclusion seems to be more plausible on two accounts. First, the NMR-derived model of the tetrameric complex predicts an interaction between the loop containing Lys^{63} of the acceptor Ub and a channel above the active site on Ubc13 (*26*). Second, a Ubc13 $Asp^{81}Ala$ substitution situated in this channel attenuates the affinity of the heterodimer for Ub *in vitro* (*25*). Therefore, Ubc13 apparently serves three key catalytic functions in Lys^{63} chain assembly: (i) the formation of thiolester with donor Ub, (ii) the orientation of Lys^{63} on the acceptor Ub toward the active site, and (iii) the concomitant increased affinity for acceptor Ub.

Mms2 and Ubc13 can be chromatographically copurified as a heterodimer which remains stable over a wide variety of concentrations and buffer conditions (*24*, *26*, *27*). The *Saccharomyces cerevisiae* homologues of these proteins also form a stable 1/1 heterodimer (*20*) with a K_D of 0.4 μM (*22*). Unfortunately, the quality of the data precluded the rigorous

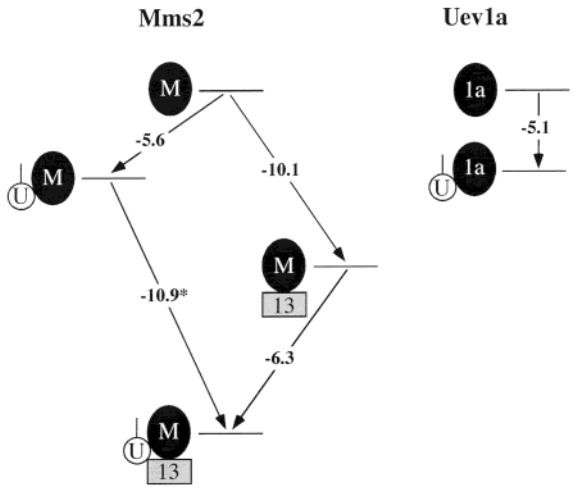

FIGURE 6: Schematic view of the relative free energies ($\Delta G°_{binding}$ in kilocalories per mole) involved in the binding of acceptor Ub by the Uev•Ubc13 heterodimer. The free energies are calculated from the NMR and ITC-derived K_D values ($\Delta G°_{binding} = RT \ln K_D$), with the exception of the $\Delta G°_{binding}$ value for the association of Mms2•Ub with Ubc13 (asterisk), which was calculated on the basis of the coupling with other free energies in the cycle: U, Ub; M, Mms2; 13, Ubc13; and 1a, Uev1a.

kinetic analysis for the Ubc13•Mms2 heterodimer interaction by 2D $^1H-^{15}N$ HSQC NMR titration experiments. However, using [^{15}N]Ubc13 and unlabeled Mms2, we were able to observe a 1/1 stoichiometry for the human proteins and estimate an upper limit of 1 μM for the value of K_D. This result is in good agreement with the previous value of 2 μM determined by analytical ultracentrifugation. To accurately determine the affinity of interaction, ITC experiments were performed, and yielded a K_D value of 49 $\pm$ 7 nM for the interaction, indicative of a tight binding event. The *in vivo* outcome of the difference in the K_D values for the yeast and human heterodimers has not been explored. The free energies associated with each of the interactions between Ub and the Mms2•Ubc13 heterodimer are summarized in Figure 6. The $\Delta G°$ for binding of Ub and Mms2 equals -5.6 kcal/mol, whereas $\Delta G°$ equals -6.3 kcal/mol for binding of the heterodimer and acceptor Ub. On the basis of our previous model for the Ub_2•Mms2•Ubc13 heterodimer, we propose that the increased affinity of acceptor Ub for Mms2 within the heterodimer compared to the interaction between Ub and Mms2 alone results predominantly from the direct binding of a loop from Ub containing Lys^{63} to Ubc13. A $\Delta G°$ of -10.1 kcal/mol was determined for the Ubc13•Mms2 interaction, and the hypothetical association of Ubc13 with the Mms2•Ub complex would result in a $\Delta G°$ of -10.9 kcal/mol. This thermodynamic cycle implies that Ubc13 binding to Mms2 likely precedes the interaction with the acceptor Ub molecule, serving to increase the affinity of Mms2 (within the heterodimer) for Ub. These results are consistent with previous biochemical studies that have shown that thiolester formation proceeds at different rates depending on the heterodimerization state of the Uev proteins (*27*).

This study, in combination with a wealth of structural information regarding catalysis of poly-Ub chain formation facilitated by the Uev•Ubc13 heterodimer, represents an important first step in understanding the thermodynamic and kinetic aspects associated with poly-Ub chain formation. We are hopeful establishment of a solid structural, thermody-

[2] T. Moraes, personal communication (2003).

namic, and kinetic base of knowledge with respect to Lys^{63}-linked chain formation will lead to more general insights into the mechanism of poly-Ub chain formation.

ACKNOWLEDGMENT

We thank Susan Smith for secretarial assistance, Linda Saltibus for technical assistance, and all of the members of the Ellison and Spyracopoulos labs for their valuable input and assistance. We thank Professor Brian D. Sykes for software and helpful discussions. We thank Professor Lewis E. Kay for pulse sequences, Deryck Webb for spectrometer maintenance, and Yanni Batsiolas and Robert Boyko for computer expertise. We also thank Landon Pastushok for plasmid construction.

REFERENCES

1. Peters, J.-M., King, R. W., and Deshaies, R. J. (1998) *Ubiquitin and the Biology of the Cell*, Plenum Press, New York.
2. Chen, Z. J., Parent, L., and Maniatis, T. (1996) *Cell 84*, 853−862.
3. Deng, L., Wang, C., Spencer, E., Yang, L., Braun, A., You, J., Slaughter, C., Pickart, C., and Chen, Z. J. (2000) *Cell 103*, 351−361.
4. Jentsch, S., McGrath, J. P., and Varshavsky, A. (1987) *Nature 329*, 131−134.
5. Hoege, C., Pfander, B., Moldovan, G. L., Pyrowolakis, G., and Jentsch, S. (2002) *Nature 419*, 135−141.
6. Finley, D., Bartel, B., and Varshavsky, A. (1989) *Nature 338*, 394−401.
7. Hicke, L., and Riezman, H. (1996) *Cell 84*, 277−287.
8. Glickman, M. H., and Ciechanover, A. (2002) *Physiol. Rev. 82*, 373−428.
9. Hochstrasser, M. (1996) *Annu. Rev. Genet. 30*, 405−439.
10. Hicke, L. (2001) *Nat. Rev. Mol. Cell Biol. 2*, 195−201.
11. Pickart, C. M. (2000) *Trends Biochem. Sci. 25*, 544−548.
12. Chau, V., Tobias, J. W., Bachmair, A., Marriott, D., Ecker, D. J., Gonda, D. K., and Varshavsky, A. (1989) *Science 243*, 1576−1583.
13. Arnason, T., and Ellison, M. J. (1994) *Mol. Cell. Biol. 14*, 7876−7883.
14. Johnson, E. S., Ma, P. C., Ota, I. M., and Varshavsky, A. (1995) *J. Biol. Chem. 270*, 17442−17456.
15. Spence, J., Sadis, S., Haas, A. L., and Finley, D. (1995) *Mol. Cell. Biol. 15*, 1265−1273.
16. Baboshina, O. V., and Haas, A. L. (1996) *J. Biol. Chem. 271*, 2823−2831.
17. Koegl, M., Hoppe, T., Schlenker, S., Ulrich, H. D., Mayer, T. U., and Jentsch, S. (1999) *Cell 96*, 635−644.
18. Wang, C., Deng, L., Hong, M., Akkaraju, G. R., Inoue, J., and Chen, Z. J. (2001) *Nature 412*, 346−351.
19. Broomfield, S., Chow, B. L., and Xiao, W. (1998) *Proc. Natl. Acad. Sci. U.S.A. 95*, 5678−5683.
20. Hofmann, R. M., and Pickart, C. M. (2001) *J. Biol. Chem. 276*, 27936−27943.
21. Brusky, J., Zhu, Y., and Xiao, W. (2000) *Curr. Genet. 37*, 168−174.
22. Ulrich, H. D. (2003) *J. Biol. Chem. 278*, 7051−7058.
23. Hofmann, R. M., and Pickart, C. M. (1999) *Cell 96*, 645−653.
24. Moraes, T. F., Edwards, R. A., McKenna, S., Pastushok, L., Xiao, W., Glover, J. N., and Ellison, M. J. (2001) *Nat. Struct. Biol. 8*, 669−673.
25. VanDemark, A. P., Hofmann, R. M., Tsui, C., Pickart, C. M., and Wolberger, C. (2001) *Cell 105*, 711−720.
26. McKenna, S., Moraes, T., Pastushok, L., Ptak, C., Xiao, W., Spyracopoulos, L., and Ellison, M. J. (2003) *J. Biol. Chem. 278*, 13151−13158.
27. McKenna, S., Spyracopoulos, L., Moraes, T., Pastushok, L., Ptak, C., Xiao, W., and Ellison, M. J. (2001) *J. Biol. Chem. 276*, 40120−40126.
28. Kay, L. E., Keifer, P., and Saarinen, T. (1992) *J. Am. Chem. Soc. 114*, 10663−10665.
29. Zhang, O., Kay, L. E., Olivier, J. P., and Forman-Kay, J. D. (1994) *J. Biomol. NMR 4*, 845−858.
30. Delaglio, F., Grzesiek, S., Vuister, G. W., Zhu, G., Pfeifer, J., and Bax, A. (1995) *J. Biomol. NMR 6*, 277−293.
31. Johnson, B. A., and Blevins, R. A. (1994) *J. Chem. Phys. 29*, 1012−1014.
32. McKay, R. T., Tripet, B. P., Hodges, R. S., and Sykes, B. D. (1997) *J. Biol. Chem. 272*, 28494−28500.
33. Williams, T. C., Shelling, J. G., and Sykes, B. D. (1985) in *NMR in the Life Science* (Bradbury, A. M., and Nicolini, C., Eds.) pp 93−104, Plenum Press, New York.
34. Wolfram, S. (1996) *The Mathematica Book*, 3rd ed., Wolfram Media/ Cambridge University Press, Cambridge, U.K.
35. Sutherland, I. O. (1971) *Annual Reports on NMR Spectroscopy*, Vol. 4, Academic Press, New York.
36. Zuiderweg, E. R. (2002) *Biochemistry 41*, 1−7.
37. Mercier, P., Li, M. X., and Sykes, B. D. (2000) *Biochemistry 39*, 2902−2911.
38. Pornillos, O., Alam, S. L., Rich, R. L., Myszka, D. G., Davis, D. R., and Sundquist, W. I. (2002) *EMBO J. 21*, 2397−2406.

BI034480T